Earth, Planets and Space

FULL PAPER Open Access

Multi-GNSS clock combination with consideration of inconsistent nonlinear variation and satellite-specific bias

Guo Chen[1], Jing Guo[1*], Na Wei[1], Min Li[1], Qile Zhao[1,2] and Jun Tao[3]

Abstract

As part of the International GNSS Service (IGS) multi-GNSS Pilot Project (MGEX), precise orbit and clock products for multi-GNSS constellations have been submitted by several analysis centers (ACs) since 2012. Based on the 30 s satellite clocks from 6 MGEX ACs, the multi-GNSS clocks are combined and the consistency of the AC clocks is assessed in this study. Usually, a linear transformation between the combined and AC solution is used for clock combination, and the clock residuals of the AC solution w.r.t the combined solution are used to determine the weights of the AC. However, any inconsistent satellite-specific bias or nonlinear variations in the clocks induced by the AC's processing strategy can contaminate the linear transformation as well as the determination of the weight. In this study, the analysis center and satellite-specific bias (ASB) of the MGEX AC clock solutions is first identified and estimated by using observations from globally distributed stations. Moreover, the clock solutions with nonlinear variations induced by the reference clock or nonconstant intersystem bias (ISB) are corrected by aligning the clocks to the selected reference solution before clock combination. With the correction of the ASB, the root-mean-square of the clock residuals decreases significantly and reaches 14—26, 37—91, 33—48 and 12—44 ps for GPS, GLONASS, BDS-2 and Galileo, respectively. In general, the consistency of AC solutions w.r.t the combination reaches 8—16, 27—58, 13—27 and 9—36 ps for GPS, GLONASS, BDS-2 and Galileo in terms of the standard deviation. Finally, the individual AC and combined orbit as well as clock solutions of different constellations are assessed by precise point positioning, and the combined multi-GNSS solutions show competitive performance with the best AC solution in terms of both the positioning accuracy and stability of the reference frame parameters. However, inconsistent scale parameters of both the AC and combined solutions are identified and require more investigation.

Keywords: Multi-GNSS, Satellite clock combination, Analysis center and satellite-specific bias, Inconsistent nonlinear variation, Reference frame parameters

*Correspondence: jingguo@whu.edu.cn

[1] GNSS Research Center, Wuhan University, No. 129 Luoyu Road, Wuhan 430079, China
Full list of author information is available at the end of the article

Graphical Abstract

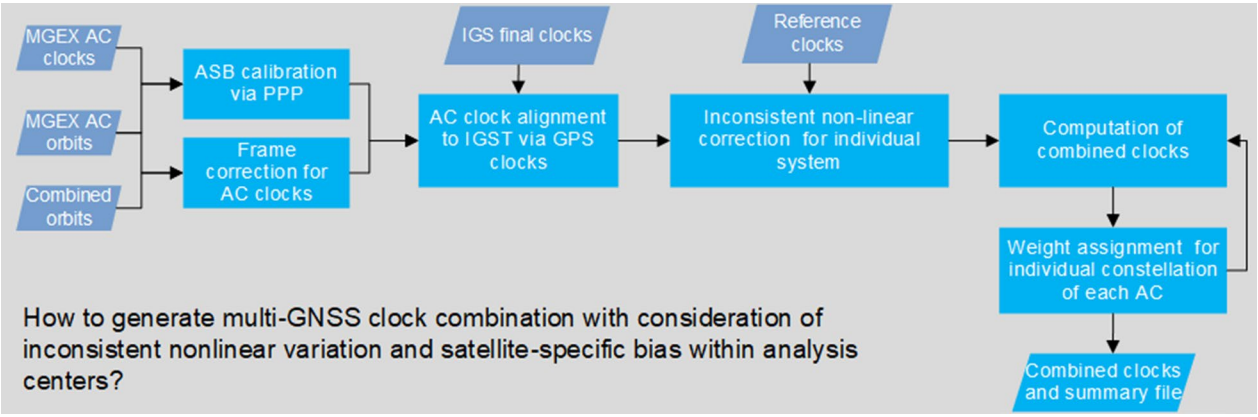

Introduction

Precise Point Positioning (PPP) with a single receiver can provide positioning with centimeter-to-millimeter accuracy globally (Zumberge et al. 1997; Kouba and Héroux, 2001; Zhao et al. 2021). Precise orbit and clock solutions are the prerequisites of PPP and can be obtained from the International GNSS Service (IGS) (Dow et al. 2009) as well as its analysis centers (ACs). Currently, only the combined orbit and clock solutions of GPS as well as orbits of GLONASS are provided by IGS. Although the development of the European Galileo, China BeiDou Satellite Navigation System (BDS), and other constellations have noticeably increased the number of satellites in space and the performance of the positioning, navigation and timing (PNT) service, combined solutions, particularly for clocks, are lacking.

IGS has already made considerable effort to improve GNSS combined solutions in terms of precision, consistency and robustness. In early 1993, the GPS orbits and Earth Orientation Parameters (EOPs) from seven ACs were collected to validate the feasibility of orbit combination (Springer and Beutler 1993). Combined GPS orbits, as IGS legacy products, have been available since 1994, and orbit comparison has also pushed forward AC improvements not only in strategy, but also in dynamic and observational models (Beutler et al. 1994, 1995; Griffiths 2019). Motived by the competitiveness of GPS orbit combination, and to meet the satellite clock requirement for precise navigation, GPS clock products were also combined by IGS (Kouba et al. 1995). To meet the demand of high-rate satellite clocks (e.g., orbit determination of low-earth-orbit spacecraft), 30-s GPS satellite clocks were submitted by ACs, and their combination is supported by IGS using a new program based on an improved strategy (Kouba 2000; Kouba and Springer 2001). The combination of AC station clocks is also allowed in the new clock combination program for the development of a stable time scale (i.e., IGS Time) together with satellite clocks (Ray 1999; Petit and Arias 2009).

In contrast to the orbits constrained by dynamic models, satellite clock estimates are prone to possible discontinuities and outliers caused by unmodeled observation errors and high correlations between clocks and phase ambiguities. Moreover, inconsistent attitude modes, especially for satellites during the eclipse season adopted by ACs, can result in inconsistency. This issue was investigated by Loyer et al. (2017), and ACs are encouraged to provide the quaternions of satellite attitudes used in precise orbit and clock determination (Loyer et al. 2021). In addition, the phase center corrections used by ACs can generate clock inconsistencies between ACs. Currently, the GPS clock combination conducted by the IGS analysis center coordinator (ACC) based on the strategy proposed by Kouba and Springer (2001) generally consists of four steps: (1) the alignment of individual AC clock solutions to the IGS reference frame with correction of the orbital errors as well as origin offset; (2) alignment of the individual ACs' clocks to a common reference time frame for the rapid convergence of the clock combination; (3) combination using an iterative outlier detection and rejection scheme based on weighted averages, with the weights determined by the absolute values of AC deviations with respect to the average; (4) realignment of the combined clocks to the IGS time scale (Kouba and Springer 2001). When the clocks are aligned to the reference time scale in steps (2) and (3), it is assumed that the clock differences between the two solutions vary

linearly. As the variations of the selected reference clock are absorbed by the clock estimates, the potential inconsistent nonlinear variation induced by the reference clock should be corrected before clock combination.

Following the success of GPS clock combination as well as the development of the multi-GNSS system, clock combination for multi-GNSS has attracted much interest from the GNSS community. The first proposal was the combination of GLONASS clocks. Unlike with GPS, the Frequency Division Multiple Access approach is used by GLONASS, and the inter-frequency code bias (IFCB) hinders the consistent combination of GLONASS clocks. To overcome this, Song et al. (2014) introduced an additional constant parameter in clock combination to reduce significant differences in the analysis center and satellite-specific bias (ASB). The day boundary discontinuity was obviously reduced even when equal weights were used for ACs to generate combined solutions (Song et al. 2014). The ASB in GLONASS clock products was also analyzed by Chen et al. (2017), and a robust least-squares estimation for clock combination was proposed. Beyond GLONASS, the ACs within the International GNSS Monitoring and Assessment System (iGMAS) have already provided global quad-constellation orbit and clock solutions, and the urgent need for combined solutions makes weighted averaging orbit and clock solutions possible (Chen et al. 2015). On the other hand, orbit and clock combination for multi-GNSS is also being undertaken by IGS, and experimental multi-GNSS combined orbits were first released at https://igs.org/acc/experimental-Multi-GNSS-combinations (Sakic et al. 2018; Masoumi and Moore. 2019; Sośnica et al. 2020). However, the orientation correction with respect to the operational IGS reference frame is not applied during multi-GNSS orbit combination (https://igs.org/acc/experimental-Multi-GNSS-combinations). With the development of PPP with Integer Ambiguity Resolution (PPP-AR), the correlation of clocks and phases as well as code biases has been achieved (Geng et al. 2019), and the PPP-AR working group was established in 2018 by the IGS Workshop at Wuhan; it is in charge of the combination of clocks as well as phase biases. An experimental combination based on satellite clock and phase bias products from six ACs over a week was conducted by IGS (Banville et al. 2020), and the strategy used was summarized in detail by Pan (2021). In addition to the combination in post-mode, to satisfy the needs of available and reliable real-time ephemeris corrections, two kinds of combined orbits and clocks are also provided by IGS based on the weighted average and Kalman filter (Mervart and Weber 2011).

For the experimental multi-GNSS combined clocks, the IGS mainly focuses on the simultaneous combination of clocks and code/phase bias products to advance the PPP with ambiguity resolution (Banville et al. 2020). However, the clock differences between two solutions (e.g., the AC and combined clocks) are assumed to vary in a linear pattern during clock combination, which is not always the case for multi-GNSS clocks. In this study, we focus on clock combination in postprocess mode for a multi-GNSS constellation based on products from IGS MGEX ACs, with consideration of ASB and nonlinear variation in clock solutions. Following the description of IGS MGEX clock products from each AC, the algorithms for multi-GNSS clock combination are presented. Subsequently, the consistency of an individual AC clock solution is assessed. Furthermore, the performance of combined orbit/clock solutions is evaluated by PPP with 96 selected globally distributed reference stations, and the accessible terrestrial reference frame parameters with respect to the IGS frame are also analyzed. Finally, the study is summarized.

Data and multi-GNSS clock combination strategy

This section starts with the collection and overview of multi-GNSS orbit/clock products of ACs. Then, the strategy for clock combination is presented with a focus on the a priori correction, inconsistent ASB and nonlinear variations. In addition, the weighting for individual constellations is designed.

MGEX orbit and clock products

IGS initiated the MGEX to track, collate and analyze all available GNSS signals (Montenbruck et al. 2017). Currently, 7 ACs are officially providing solutions for multi-GNSS constellations, i.e., the Centre National d'Etudes Spatiales/Collecte Localisation Satellites (CNES/CLS), the Center for Orbit Determination in Europe (CODE), Deutsches GeoForschungsZentrum Potsdam (GFZ), the Information and Analysis Center (IAC), the Japan Aerospace Exploration Agency (JAXA), Shanghai Observatory (SHAO), and Wuhan University (WHU). In addition, the European Space Agency (ESA) releases multi-GNSS solutions on its own server. In this study, the orbit and clock products from CNES/CLS, CODE, ESA, GFZ, JAXA, and WHU over the whole year of 2018 are collected for clock combination and positioning. As IAC began to submit solutions in the second half of 2020 and the sampling rate of clock solutions is 300 s for SHAO while it is 30 s for other ACs, these two ACs are excluded from clock combination.

Table 1 lists the status of the multi-GNSS orbit and clock products used for clock combination. There are 4 ACs, i.e., CODE, ESA, GFZ and WHU, providing precise orbit and clock products for five constellations (i.e., GPS, GLONASS, BDS, Galileo and QZSS). However, the GEO

Table 1 Overview of orbit and clock products from the selected ACs for clock combination. 'G' 'R', 'C', 'E', and 'J' in the fourth column indicate GPS, GLONASS, BDS, Galileo and QZSS, respectively

AC	ID for multi-GNSS clock combination	Intervals of orbit/clock products	Constellation	Clock types
CNES/CLS	GRM	5 min/30 s	GRE	Integer recovery clocks
CODE	COM	5 min/30 s	GRECJ	Common clock for GPS and Galileo since mid-2018, code clock for the rest (Schaer et al. 2021)
ESA	ESM	5 min/30 s	GRECJ	Code clock
GFZ	GFM	5 min/30 s	GRECJ	Code clock
JAXA	JAM	5 min/30 s	GRJ	Code clock
WHU	WUM	15 min/30 s	GRECJ	Code clock

satellites of BDS are not included in the CODE and ESA products. In addition to GPS and GLONASS, the satellite orbit and clock of Galileo and QZSS are supported by CNES/CLS and JAXA, respectively. As only a regional BDS constellation (BDS-2) was available from those ACs in 2018, only BDS-2 is analyzed in this study. Integer clocks are provided by CNES/CLS, whereas the other ACs' clocks are similar to those of the IGS legacy clock.

Multi-GNSS clock combination

For clock combination, the AC raw clock solution $C_{a0}^{s,i}$ can be expressed as

$$C_{a0}^{s,i} = C^{s,i} + B_a - ASB_a^{s,i} + \mathrm{d}_{a,cor}^{s,i}, \tag{1}$$

where $C^{s,i}$ is the sum of real physical clock offset and common hardware delays including the time-invariant part of code/phase hardware delays and the time-varying phase hardware delays, which is common for all ACs clocks. The superscript s and i indicate satellite i of constellation s. B_a is the AC-specific time scale, which is usually taken from a selected station clock to avoid rank deficiency during clock determination. $d_{a,cor}^{s,i}$ is the a priori correction applied before clock combination to compensate for the inconsistency between AC and combined orbits. Generally, $d_{a,cor}^{s,i}$ includes corrections for inconsistent frames (i.e., $d_{a,frm}^{s,i}$), attitude mode ($d_{a,att}^{s,i}$) and phase center offset ($d_{a,pco}^{s,i}$), which are subsequently substituted with $d_{a,cor}^{s,i} = d_{a,frm}^{s,i} + d_{a,att}^{s,i} + d_{a,pco}^{s,i}$. $ASB_a^{s,i}$ is the AC and satellite-specific bias, which is not common within different AC, and possibly induced by the AC's processing strategy (e.g., inconsistent observation networks with mixed receivers used for ACs).

A priori correction for AC clocks

To maintain the consistency between the combined orbit and clock, the following formula proposed by Ferland (1999) is adopted for the frame correction of individual AC clock:

$$d_{a,frm}^{s,i} = \frac{O_a^{s,i} \cdot \left(O_a^{s,i} - O_{cmb}^{s,i} - DX_a\right)}{c \cdot R^{s,i}} \tag{2}$$

where the superscripts s and i indicate the constellation and satellite, respectively; $\boldsymbol{O}_a^{s,i}$ and $\boldsymbol{O}_{cmb}^{s,i}$ represent AC a and the combined orbits, respectively; $R^{s,i}$ is the distance of the satellite in the Earth-Centered-Earth-Fixed (ECEF) coordinate system; c is the velocity of light; and $\boldsymbol{DX}_a$ is the geo-center offset obtained by comparing the AC station coordinates with respect to the combination. Considering that not all AC station coordinates are available during the combination experiment, no geo-center correction is applied for AC clock solutions.

To analyze the impacts of frame correction on clock combination, the clock differences between the two solutions are derived with the following formula:

$$\nabla C_{a,b}^{s,i} = (C_a^{s,i} - C_b^{s,i}) - \frac{1}{n}\sum_{j=1}^{n}\left(C_a^{s,j} - C_b^{s,j}\right). \tag{3}$$

Figure 1 shows the inter-satellite and inter-AC clock differences of ESM and COM solutions without and with frame correction for the first day in 2018. It is demonstrated that the nonlinear variations in double differenced clock induced by different orbit errors are significantly reduced once frame correction is applied. Compared to the differences without frame correction, the mean standard derivation (STDev) of the clock residuals is reduced to 0.049, 0.082, 0.026 and 0.037 ns from 0.088, 0.111, 0.233 and 0.099 ns for GPS, GLONASS, BDS-2 and Galileo, respectively. It also indicates that performing a quality assessment of clock products by using the approach of Eq. (3) regardless the frame correction is not rational, especially for newly established constellations (e.g., BDS and Galileo).

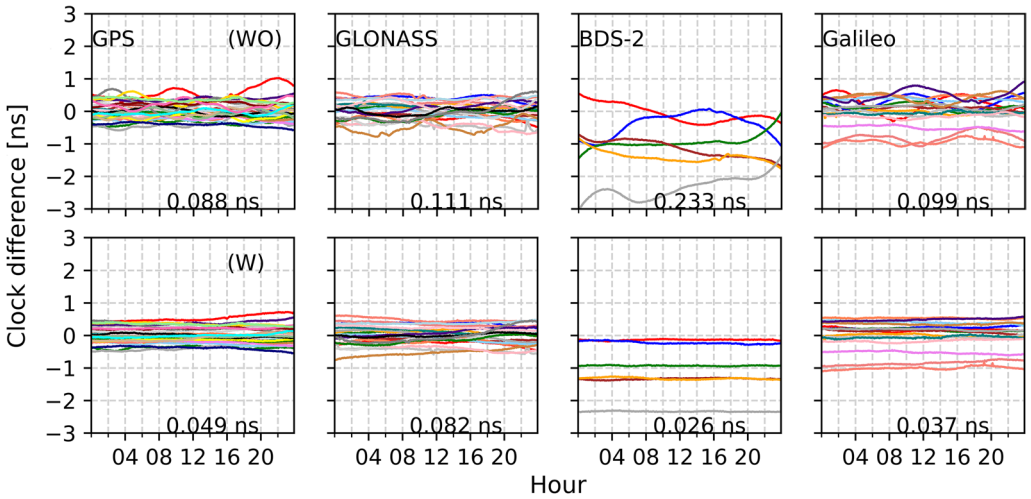

Fig. 1 Inter-satellite and inter-AC clock differences of the ESM and COM solutions without (WO) and with (W) the frame correction for the first day of 2018. Different colors are used for line plots to indicate individual satellites and the values in black are the mean STDevs for each constellation

Corrections induced by inconsistent attitude modes and phase center offsets (PCOs) are obtained from Eqs. (4) and (5), respectively:

$$d^{s,i}_{a,att} = \frac{\left(\emptyset^{s,i}_{a} - \emptyset^{s,i}_{ref}\right)}{2\pi \cdot f^{s,i}}, \tag{4}$$

$$d^{s,i}_{a,pco} = -\frac{\left(PCO^{s,i}_{a,Z} - PCO^{s,i}_{ref,Z}\right)}{c}, \tag{5}$$

where $\varnothing^{s,i}_{a}$ and $\varnothing^{s,i}_{ref}$ are the yaw angles of the AC and the reference value, respectively. $f^{s,i}$ is the frequency of ionosphere-free combination (Loyer et al. 2021). $PCO^{s,i}_{a,Z}$ and $PCO^{s,i}_{ref,Z}$ are the Z-PCO values of the individual AC and the reference AC, respectively.

Because the PCO values are described in the satellite body fixed system, a minus sign is added in Eq. (5). Since the attitude products are not available for any ACs during the clock combination period of 2018, the correction of $d^{s,i}_{a,att}$ is not applied for AC clock solutions. For the GPS and GLONASS PCOs, conventional values from the IGS ATX file are adopted by all ACs, and there is no need to consider $d^{s,i}_{a,pco}$ for these two constellations (i.e., $d^{s,i}_{a,pco} = 0$). For the BDS and Galileo constellations, there are some discrepancies among ACs during the combination period. For example, ESA and WHU adopted the PCO values of BDS-2 from the self-calibration, while the PCOs from IGS ATX were used for other ACs. There is a small difference between the Galileo PCO values adopted by CODE and by IGS ATX. It is also noted that $d^{s,i}_{a,pco}$ is linearly related to $ASB^{s,i}_{a}$ and can be calibrated simultaneously.

Analysis center and satellite-specific bias correction

Obvious ASBs in the clock residuals after frame correction are noticed in Fig. 1 and would contaminate the combined results. Because different observation networks with mixed receivers are used for ACs, the ASBs induced by the pseudorange noises, hardware delays and signal distortions are inconsistent among ACs.

In this study, we calibrate the ASB as a daily constant using an identical software package and observations from a global network. Using the precise products from the AC, the ionosphere-free observation accounting for the ASB parameter can be expressed by

$$P^{s,i}_{IF,r} = \rho^{s,i}_{r} + cd_r - cC^{s,i}_{a0} - cASB^{s,i}_{a} + ISB^{s0_s}_{r} + T^{s,i}_{r} + \varepsilon^{s,i}_{P_{IF},r}, \tag{6}$$

$$L^{s,i}_{IF,r} = \rho^{s,i}_{r} + cd_r - cC^{s,i}_{a0} - cASB^{s,i}_{a} + ISB^{s0_s}_{r} + T^{s,i}_{r} + \lambda^{s}_{IF}N^{s,i}_{r} + \varepsilon^{s,i}_{L_{IF},r}, \tag{7}$$

where $P^{s,j}_{IF,r}$ and $L^{s,j}_{IF,r}$ are the ionosphere-free pseudorange and phase measurements, respectively, and $\varepsilon^{s,i}_{P_{IF},r}$ and $\varepsilon^{s,i}_{L_{IF},r}$ are the observation noises. $\rho^{s,j}_{r}$ is the geometric distance between satellite i and station r with the correction of relativistic, tidal loading and phase center offset. d_r is the receiver clock including the real physical clock offset and time scale B_a. Considering that the $C^{s,i}_{a0}$ is consistent with the orbit of AC a, no frame correction is employed for $C^{s,i}_{a0}$. $ISB^{s0\_s}_{r}$ is the daily constant intersystem bias (ISB) between systems s and $s0$ (i.e., GPS). $T^{s,i}_{r}$ is the tropospheric delay. λ^{s}_{IF} and $N^{s,i}_{r}$ are the wavelength and ambiguity of the ionosphere-free phase, respectively.

For the estimation of ASB, 96 globally distributed stations with the capacity to track multi-GNSS signals are

selected, as shown in Fig. 2. The 300 s dual-frequency code and phase measurements of L1 and L2 for GPS, as well as QZSS, G1 and G2 for GLONASS, B1I and B2I for BDS-2, and E1 and E5a for Galileo, are used to conduct float PPP in static mode. The satellite orbits and clocks are held fixed with AC products, and to separate the ASB, ISB and receiver clock, the sum of the ASB for all satellites in each constellation is constrained as zero. The IGS antenna file (i.e., igs_2136.atx) is adopted to correct the phase center variation, and any inconsistency in phase center values between AC and IGS antenna files is absorbed by the estimates of the ASB.

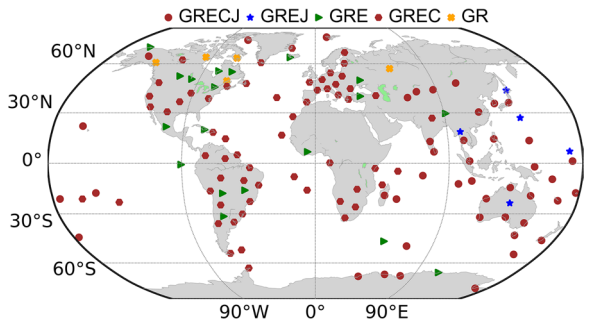

Fig. 2 Distribution of global stations used for ASB calibrations of individual AC clock products. These stations are also used for PPP validation with combined orbit and clock solutions. The abbreviations 'G', 'R', 'C', 'E' and 'J' indicate GPS, GLONASS, Galileo, BDS and QZSS, respectively

Figure 3 illustrates the ASB difference and daily bias of double differenced clock with respect to COM solutions for the first day in 2018, and the correlations are also presented. Due to the fact the number of satellites for ASB constraint are different among ACs, an average bias of all satellites is removed from the ASB difference of each constellation. As only three constellations are available for GRM and JAM, their results are not shown here. It is noticed that most of the ASB differences for GPS and Galileo satellites are within 1.0 ns, whereas those of GLONASS and BDS-2 satellites are scattered across larger values, and the maximum can reach more than 3.0 ns for some satellites. A high correlation between the clock and ABS difference can be identified, and the correlation coefficients for each constellation are larger than 0.95 for all ACs. Hence, the ASBs estimated based on the proposed approach can be used to calibrate the clock solutions.

Inconsistent nonlinear variation of clocks

With a priori correction as well as ASB bias calibration, the corrected clock solution $C_{a1}^{s,i}$ for satellite i of AC a can be obtained as

$$C_{a1}^{s,i} = C_{a0}^{s,i} + ASB_{a}^{s,i} - \mathrm{d}_{a,cor}^{s,i} = C^{s,i} + B_a \tag{8}$$

where $C_{a0}^{s,i}$ is the raw clock solution; B_a is the AC-specific time scale, which is common to all satellites and usually

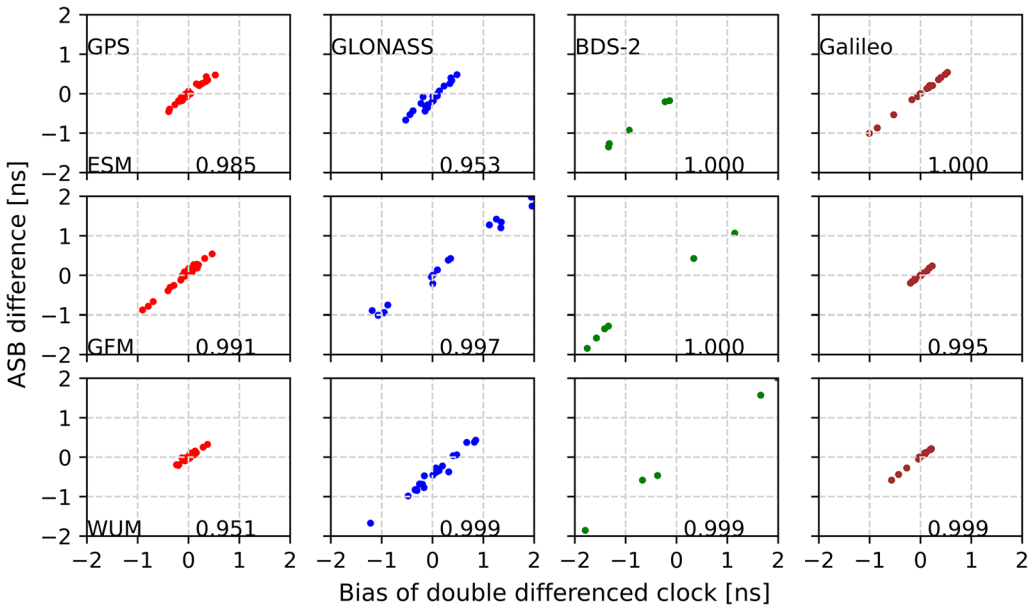

Fig. 3 Correlations between the bias of double differenced clock and ASB for satellites of each constellation with respect to COM on DOY 001, 2018. The values in black are the correlation coefficients

depends on the reference clock, e.g., a single receiver or satellite clock, used by the AC.

Considering that the B_a of the clock solution may be arbitrary, it is necessary to keep B_a compatible with different constellations. To analyze the time scale of individual ACs, the single difference between ACs of a and b can be obtained with the following formula:

$$\nabla C^{s,i}_{a1,b1} = \nabla C^{s,i}_{a,b} + \nabla B_{a,b}, \tag{9}$$

where ∇ represents the single difference operator. Since $C^{s,i}$ is only related to satellites, $\nabla C^{s,i}_{a,b}$ can be canceled. Assuming that B_a is only an AC-specific parameter, and since stations equipped with stable atomic clocks are usually used as reference stations, the difference $\nabla B_{a,b}(t)$ at epoch t can be fitted by a linear model:

$$\nabla B_{a,b} = \nabla O_B + \nabla D_B * \Delta t, \tag{10}$$

where ∇O_B and ∇D_B are the intercept and drift of $\nabla B_{a,b}$, respectively, and Δt is the elapsed time between t and the reference epoch.

Figure 4 presents the GPS and GLONASS single-difference clocks of individual ACs with regard to COM for the first day of 2018, and GPS satellites are used to obtain the coefficients of the time scale difference (i.e., ∇O_B and ∇D_B). The residuals of the GPS clocks are near zero, with an STDev less than 0.15 ns, except for the JAM solution. For the GPS and GLONASS clock differences of the JAM solution, significant nonlinear but consistent variations can be observed, which are most likely induced by a clock reference station equipped with an unstable clock. It is inferred from the GLONASS clock residuals that all ACs estimate the ISB as constant except GFZ, and a temporal variation in GLONASS with a range of 3.0 ns can be observed. Meanwhile, a clock jump is noticed for satellite R21 presented as yellow line and a few outliers are also found for the GRM solution, which indicate that outlier detection and transformation parameters of piece-wise should be implemented for clock combination.

IGS usually uses a linear transformation between the AC and the combined solution in the clock combination to remove the differences in time scales among ACs (Kouba and Springer 2001). To obtain reliable weights from the clock residuals and meet the prerequisite of linear transformation for clock combination, it is essential to remove the inconsistent nonlinear variation induced by the time scale and ISB. In this study, one AC with a stable time scale and constant ISB is selected as a reference, and the inconsistent nonlinear variation in the other ACs (e.g., GFZ) is estimated with the following formula:

$$C^{s,i}_{ref} = C^{s,i}_{a} + dC^{s}_{a,nl} + O^{s}_{a} + D^{s}_{a} * \Delta t, \tag{11}$$

where $C^{s,i}_{ref}$ is the clock solution of the reference AC. $dC^{s}_{a,nl}$ is the nonlinear estimate for the AC clock solution

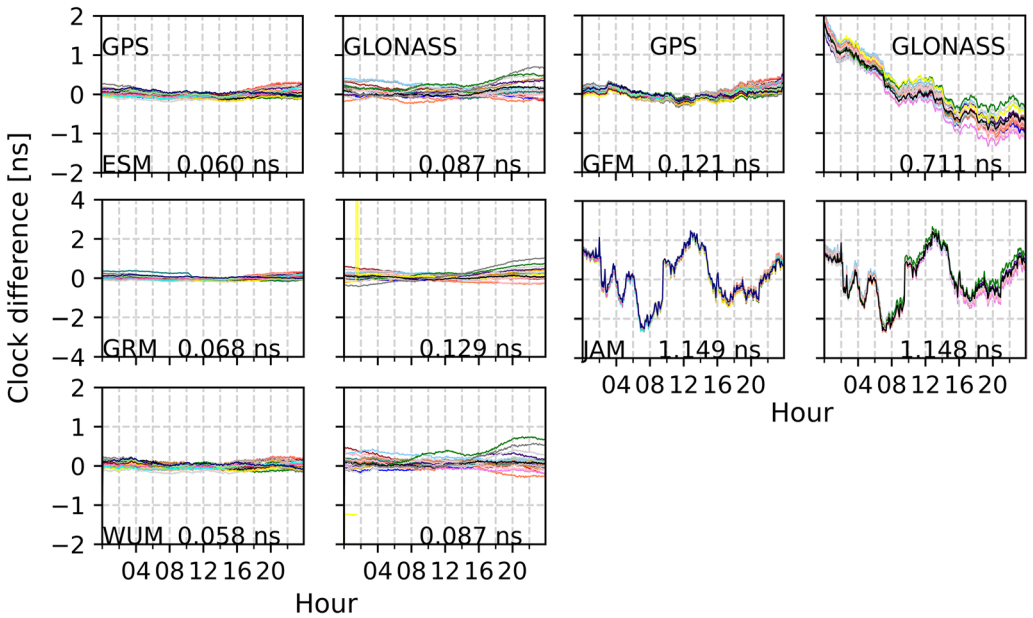

Fig. 4 Clock differences between ESM, GFM, GRM, JAM, WUM and COM for GPS and GLONASS on DOY 001, 2018. Different colors indicate different satellites and the values in black are the mean STDevs for each constellation. The average bias of all satellites is subtracted from GLONASS clock difference for clarity

of a. O_a^s and D_a^s are the bias and trend of the time scale. The estimates of $dC_{a,nl}^s$ and O_a^s in Eq. (11) are linearly correlated. To separate them, the following constraint is added at each epoch:

$$\frac{1}{n}\sum_{i=1}^{n}\left(C_{ref}^{s,i} - C_a^{s,i} - O_a^s - D_a^s * \Delta t\right) = 0, \tag{12}$$

where n is the number of common satellites for constellation s.

The clock difference of the solution GFM with regard to the COM is presented in Fig. 5 with the correction of constellation-specific nonlinear estimates using Eq. (11). It is clear that the nonlinear variations in the clock residuals disappear, and the mean STDev decreases to 0.048 and 0.076 ns from 0.121 and 0.711 ns for GPS and GLONASS, respectively. Equation (11) can also be used to align the nonlinear time scale of the JAM solution to the reference, and the STDevs of GPS and GLONASS are reduced from 1.149 to 0.048 ns and from 1.148 ns to 0.081 ns, respectively.

AC-specific weight determination for each constellation

Since the quality of the clock product depends on the processing strategies employed by individual ACs and different performances of AC clock solutions within constellations is noticed, the weight of an individual AC (i.e., w_a^s) for each constellation is determined separately by

$$w_a^s \sim \frac{1}{\left(\sigma_a^s\right)^2}, \sum w_a^s = 1, \tag{13}$$

where σ_a^s is the root-mean-square (RMS) of the clock residuals for constellation s of AC a. The clock residuals are obtained by aligning the individual AC to the combined solution as follows:

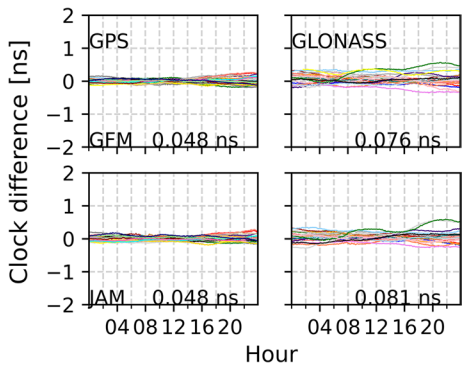

Fig. 5 Clock difference of GFM and JAM with respect to COM for GPS and GLONASS with correction of the constellation-specific nonlinear variation on DOY 001, 2018. The values in black are the mean STDevs for each constellation

$$C_{cmb}^{s,i} + v_{a2}^{s,i} = C_{a2}^{s,i} + O_{a2}^s + D_{a2}^s * \Delta t, \tag{14}$$

where $C_{cmb}^{s,i}$ is the combined clock and $C_{a2}^{s,i}$ are the AC solutions with the correction of $d_{a,frm}^{s,i}$, inconsistent ASB and nonlinear variation. O_{a2}^s and D_{a2}^s are the transformation parameters, i.e., intercept and drift of an individual constellation. $v_{a2}^{s,i}$ is the AC clock residuals compared to the combined solution.

The flowchart for multi-GNSS clock combination proposed in this study is illustrated in Fig. 6. First, ASBs are estimated using global stations and AC orbit and clock products. Afterward, the frame correction is computed by Eq. (2) and applied to the individual AC clock solution. Second, the individual solution is aligned to a common time scale to speed up the convergence of the clock combination, as proposed by Kouba and Springer (2001). In this study, the final GPS combined clock provided by IGS is selected as the reference to keep the time scale of the combined solution consistent with IGS time scale. Moreover, the inconsistent nonlinear time scale applied in the AC solution is also removed by alignment to IGS. Third, one AC with constant ISB estimates is selected as a reference, and the constellation-specific nonlinear variation is calibrated using Eqs. (11) and (12). Fourth, an iterative combination is employed to adjust the weights of the individual AC solutions until no outliers are detected or the maximum iteration number (i.e., 3) is reached, and a final combination and comparison is performed.

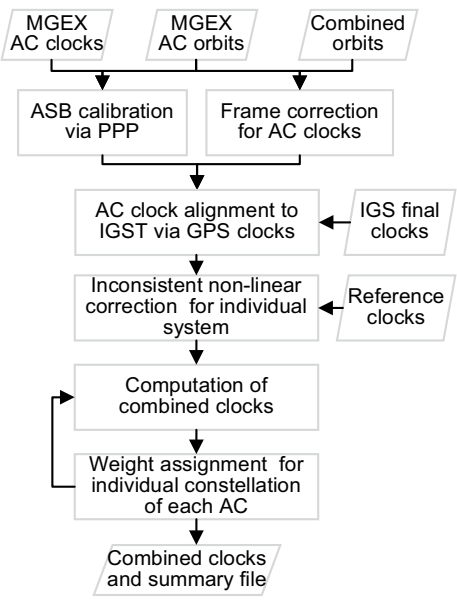

Fig. 6 Processing flowchart of multi-GNSS combined clock

Assessment of the combined clock solution

The clock solutions from the ACs are compared to the combined clocks in this section. Moreover, the observations from the global stations shown in Fig. 2, as well as individual ACs and combined orbits and clocks, are input to PANDA package for daily PPP of the whole year of 2018 (Liu and Ge 2003).

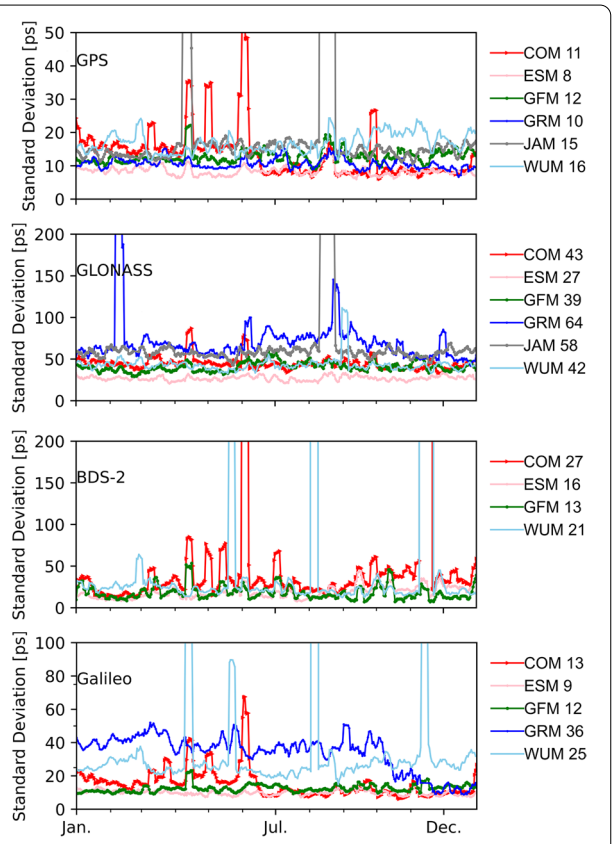

Fig. 7 STDevs of the GPS, GLONASS, BDS-2 and Galileo satellite clocks for different ACs in 2018. The daily STDevs are smoothed with a moving window with a 7-day width, and the values in the legend are the median STDevs

Consistency of multi-GNSS clocks

Figure 7 shows the daily STDev with respect to the combined solutions for each AC. For clear illustration, the daily results are smoothed using a moving window with a 7-day width. Because no more than 4 satellites are available for QZSS during the experiment, the results of QZSS are not presented. The yearly median of STDevs is also listed in the legend of Fig. 7 for each AC. For GPS, similar performances are obtained for different ACs, and the consistency between the ACs and the combined solution is in the range of 8−16 ps. An obvious decrease can be observed after 22 June 2018 for COM, and it may be caused by the ambiguous integer solution for MGEX clocks (Dach et al. 2019).

During the selected period, the STDevs of GLONASS are approximately 4 times larger than those of GPS. The ESM shows the best consistency of 27 ps, followed by GFM, WUM and COM, where the GRM and JAM solutions are approximately 60 ps for GLONASS. For BDS-2, the GEO satellites are excluded from the statistics, and the consistency of the other satellites can reach 20 ps. However, there are frequent and noticeable jumps for the BDS-2 clocks, especially for the COM solution. This could be partly caused by an inaccurate attitude and solar radiation pressure model that was used until a dedicated model was activated at the beginning of July (Dach et al. 2019).

For Galileo, the COM, ESM and GFM solutions show good consistency, with a STDev of approximately 10 ps. An obvious improvement can be seen for COM when the fixed-ambiguity clock products were generated at the end of June. The GRM solution also benefited from fixed undifferenced phase observations after 7 October 2018 (Perosanz et al. 2018), and the STDev decreased from 40 to 15 ps. The median STDev reached 25 ps for the WUM solution.

To show the validity of the ASB calibration approach proposed in this study, we recombined the clock without ASB correction. Table 2 lists the RMS values of the clock

Table 2 RMS of AC clock for different constellations compared to combination with (W) and without (WO) ASB correction. The GEO satellites are excluded from the BDS-2 solution statistics (unit: ps)

Solution	GPS		GLONASS		BDS-2		Galileo	
	W	WO	W	WO	W	WO	W	WO
COM	19	134	58	240	48	1942	17	239
ESM	14	107	37	259	33	1109	12	120
GFM	26	205	64	3522	35	348	21	309
GRM	18	119	91	2041	–	–	44	140
JAM	26	211	86	385	–	–	–	–
WUM	24	180	61	405	42	1083	30	138

residuals for different constellations with and without ASB correction. Compared to the solutions without ASB correction, the RMS of solutions with ASB correction noticeably decreases, especially for GLONASS and BDS-2. For GPS, BDS-2 and Galileo, RMS values smaller than 50 ps are achieved for AC solutions with ASB correction. The corresponding values of GLONASS are larger than the others, and the RMS is approximately 37—91 ps. The RMS of GLONASS and BDS-2 can reach a few nanoseconds for some solutions without ASB correction (i.e., COM and ESM for BDS-2, GFM and GRM for GLONASS). Generally, using the ASB correction approach proposed in this study, the RMS of clock residuals can be reduced by approximately 85—88%, 76—98%, 90—98%, and 69—93% for GPS, GLONASS, BDS-2 and Galileo, respectively.

The ASB residuals could also be used as an internal metric of validation of the ASB correction approach. First, the ASB biases are estimated for each AC with its orbit and clock products, and a combined ASB is generated by means of averaging based on different ACs. Second, the combined satellite clock solutions (i.e., W) are obtained based on the processing strategy illustrated in Fig. 6. Additionally, the combination without ASB correction applied to the AC solutions is generated (i.e., WO). Third, both the W and WO solutions are used to estimate the ASB again as in the first step, and the estimates are compared to the ASB combination. Figure 8 shows the daily RMS of the ASB residuals for each constellation. It is clear that the agreement between the ASB combination and the estimates from the W solution has a significant improvement compared to the WO solution, and the RMS decreases from 46, 100, 667, 85 ps to 19, 34, 86, 13 ps for GPS, GLONASS, BDS-2 and Galileo, respectively. This confirms the validation of ASB correction for AC solutions before clock combination.

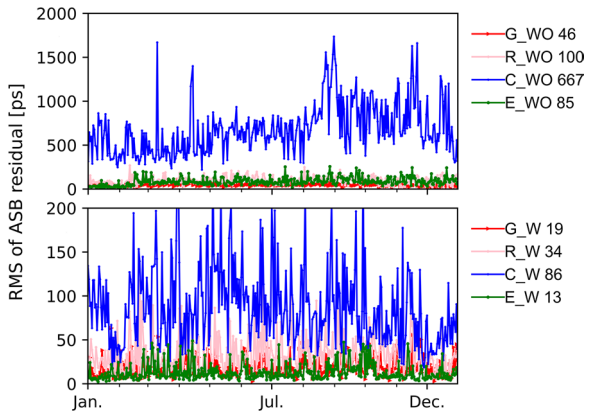

Fig. 8 Daily RMS of ASB residuals for multi-GNSS combined clock solutions with (W) and without (WO) ASB correction. 'G', 'R', 'C', 'E', and 'J' in the legend indicate GPS, GLONASS, BDS-2, and Galileo, respectively. The values in the legend indicate the median RMS

Precise point positioning with multi-GNSS combined orbit and clock

In this section, static daily PPP is performed with the combined multi-GNSS orbit and clock solutions of the whole year of 2018 for the global stations shown in Fig. 2. The PPP strategy is similar to that described for ASB estimation. It should be noted that the ASB is no longer estimated. The positions are compared to the IGS daily coordinates, and a 7-parameter Helmert transformation is applied to remove the systematic errors.

Position accuracy

To assess the combined orbit and clock consistency, Table 3 lists the statistics of position accuracy for different constellations. Due to an insufficient number of satellites, BDS-2 and QZSS-only PPP is not conducted. In general, GPS achieves the best position accuracy in the three single-constellation tests, and the average RMS reaches 0.31, 0.17 and 0.45 cm in the east, north and up components, respectively. Compared to GPS positioning, the position accuracy of GLONASS and Galileo is slightly lower. The yearly average RMS is 0.49, 0.31 and 0.69 cm in the three components for GLONASS, whereas they are 0.52, 0.40 and 0.90 cm for Galileo. Compared to the GPS-only PPP, the multi-GNSS solutions improve the accuracy by 16–26% in the east component (Table 3). Due to the high stability and accuracy of the combined orbits and clock solutions, the competitive PPP results can be obtained compared with the best AC solution.

Reference frame parameters

The consistency of the reference frame achieved by a precise orbit and clock can be evaluated by comparing the

Table 3 RMS of the east/north/up components for daily PPP using the precise orbit and clock of each analysis center as well as the combined solutions for different constellations. 'WMC' indicates the combined solutions in this study (unit: cm)

Solution	GPS	GLONASS	Galileo	All
COM	0.36/0.23/0.54	0.52/0.34/0.76	0.58/0.45/0.99	0.28/0.22/0.55
ESM	0.33/0.18/0.48	0.50/0.33/0.74	0.53/0.42/0.93	0.25/0.18/0.46
GFM	0.35/0.20/0.49	0.53/0.36/0.76	0.55/0.42/0.94	0.29/0.19/0.48
GRM	0.35/0.20/0.50	0.58/0.39/0.84	0.70/0.48/1.09	0.30/0.20/0.49
JAM	0.34/0.19/0.49	0.50/0.35/0.76	-/-/-	0.28/0.18/0.44
WUM	0.32/0.18/0.47	0.49/0.34/0.72	0.59/0.43/1.00	0.27/0.19/0.48
WMC	0.31/0.17/0.45	0.49/0.31/0.69	0.52/0.40/0.90	0.23/0.17/0.45

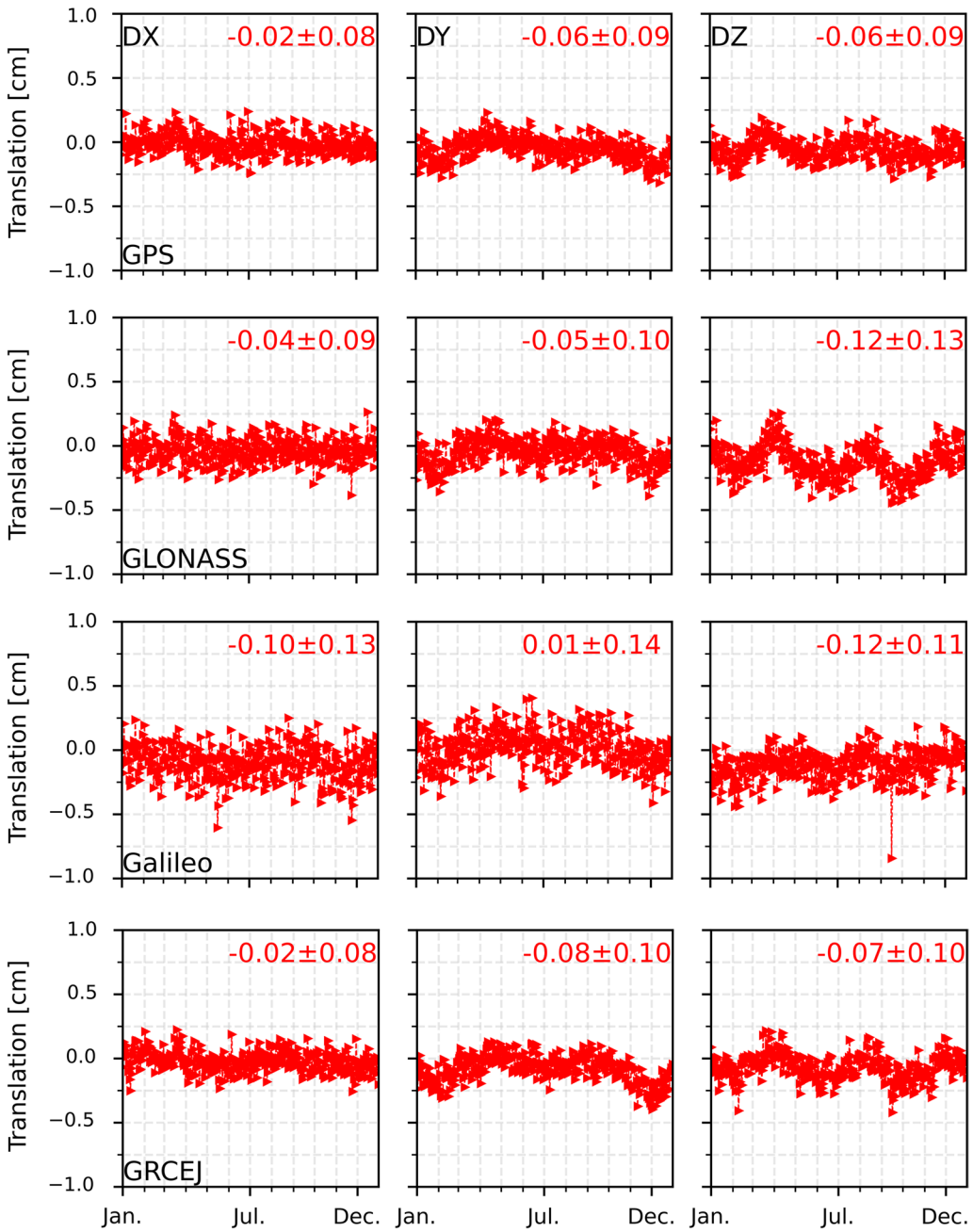

Fig. 9 Translations of the PPP solution determined with combined orbit and clock solutions with respect to the IGS daily solution. 'GRCEJ' indicates the translation of GPS, GLONASS, BDS-2, Galileo, and QZSS integrated PPP solution

transformation parameters regarding the International Terrestrial Reference Frame (i.e., IGS14). Figure 9 illustrates the translation parameters derived from PPP with a combined orbit and clock. The daily translations of PPP fall into the range of ±3mm for each constellation, and the STDevs are less than 1.5 mm for all three components. Among the single-system solutions, the translations of all components have a negative bias, except the Y-translation of Galileo. Additionally, translations derived from the combined GPS solution are more centered than those of GLONASS and Galileo. Due to the relatively high position noise of Galileo, the translations for Galileo are the most scattered. For PPP using the combined multi-GNSS orbit/clock, the translations vary similarly to those of a single GPS constellation.

The correlation coefficients within translations of different PPP solutions are computed and the coefficients are listed in Table 4. Although the translations are contaminated by the noise and lower accuracy of the position results, especially for Galileo, a moderate correlation is still seen within the translations of different constellations. Due to the contribution of individual constellations in the multi-GNSS integrated PPP, the correlation coefficients of translations between single-constellation and multi-GNSS solutions are expected to be larger than that between two constellations. The moderate correlation within translations also indicates the high consistency between the combined orbit and clock.

For the rotation parameters presented in Fig. 10, the Galileo solutions have the largest rotations, whereas those of GPS have the smallest. However, there is no obvious difference for rotations derived from PPP using the combined orbits and clocks of different constellations, and most of the daily rotations are in the range of −50 to 50 uas. Compared to the correlation coefficients of translations, a lower correlation is noticed for rotations (Table 4), which can be explained by the fact that the AC orbits are aligned to the IGS final orbit during orbit combination.

For the scale parameters demonstrated in Fig. 11, inconsistent scale biases are identified for different constellations, and the yearly averages are −0.06, 0.06 and −0.26 ppb for GPS, GLONASS and Galileo, respectively. Compared to the scales derived from GPS and GLONASS solutions, the scales for Galileo solutions are more scattered. Nevertheless, a larger correlation between Galileo and GPS solutions than that between GLONASS and GPS is obtained (i.e., 0.23 versus 0.09, Table 4).

Table 5 lists the statistics of transformation parameters of multi-GNSS integrated PPP for comparison between the ACs and combined solution (WMC). First, an offset larger than 1.0 mm is observed for some ACs, i.e., −1.8 mm (DY) for COM, 1.2 mm (DX) and −1.5 mm (DZ) for GRM, and −3.8 mm (DZ) for WUM solutions. Since the multi-GNSS combinations are dominated by ACs, it is expected that a consistent negative bias for the translations of PPP using combined orbits/clocks can be obtained. Additionally, offsets larger than 1.0 mm (i.e., 33 uas for an equatorial point with an Earth radius of 6371 km) are obtained for the RX of the GRM and the RY and RZ of the JAM. Considering that the orientation of the combined orbits is already aligned to the IGS terrestrial frame, no significant offsets are identified for the WMC solution. All the scales derived from PPP using the multi-GNSS orbits/clocks of ACs show a negative bias, which may be related to the antenna phase correction, and further study is needed. Finally, the combined multi-GNSS orbit and clock determine the robust PPP results, and the STDevs of the transformation parameters are competitive with those of the best AC.

Impact of the proposed strategy for clock combination on PPP results

To make a comparison between the combined clocks proposed in this contribution and the solutions with traditional strategy without consideration of the ASB and nonlinear variation, static and kinematic PPP with float ambiguity were conducted for the first 7 days of 2018. A least square filter was adopted to determine position of epoch by epoch with an interval of 30 s, and an initial constraint of 50 m was used for the position parameters of PPP in static and kinematic mode. Moreover, the process noise of 5 m was employed for position estimates for kinematic PPP. The estimates of ISB was taken as daily constant for multi-GNSS integrated PPP. The station coordinates from the static daily PPP were used as true values, and the positioning errors of 24 h are computed. Due to the convergence, the positioning results of the first hour were excluded for statistics. Some epochs with positioning errors larger than 5-sigma or number of satellites less than 5 were also removed.

Figures 12 and 13 demonstrate the positioning error of multi-GNSS integrated PPP in static and kinematic mode, respectively, for station STK2 during the period of January 1, 2018. An obvious bias is noticed, especially in the up component, which should be induced by the uncalibrated ASB and nonlinear variation related to time

Table 4 Correlation coefficients for the transformation parameters derived from PPP using the combined orbits and clocks. 'G', 'R', 'E', and 'A' in the first column indicate the PPP results for the GPS, GLONASS, Galileo and multi-GNSS combined solutions, respectively

Solution pairs	DX	DY	DZ	RX	RY	RZ	Scale
G-R	0.51	0.52	0.60	0.29	0.49	0.15	0.09
G-E	0.34	0.40	0.42	0.28	0.39	0.30	0.23
G-A	0.69	0.75	0.78	0.55	0.71	0.56	0.47
R-E	0.34	0.39	0.41	0.11	0.32	0.20	0.06
R-A	0.58	0.65	0.78	0.52	0.70	0.25	0.29
E-A	0.59	0.62	0.61	0.45	0.55	0.43	0.38

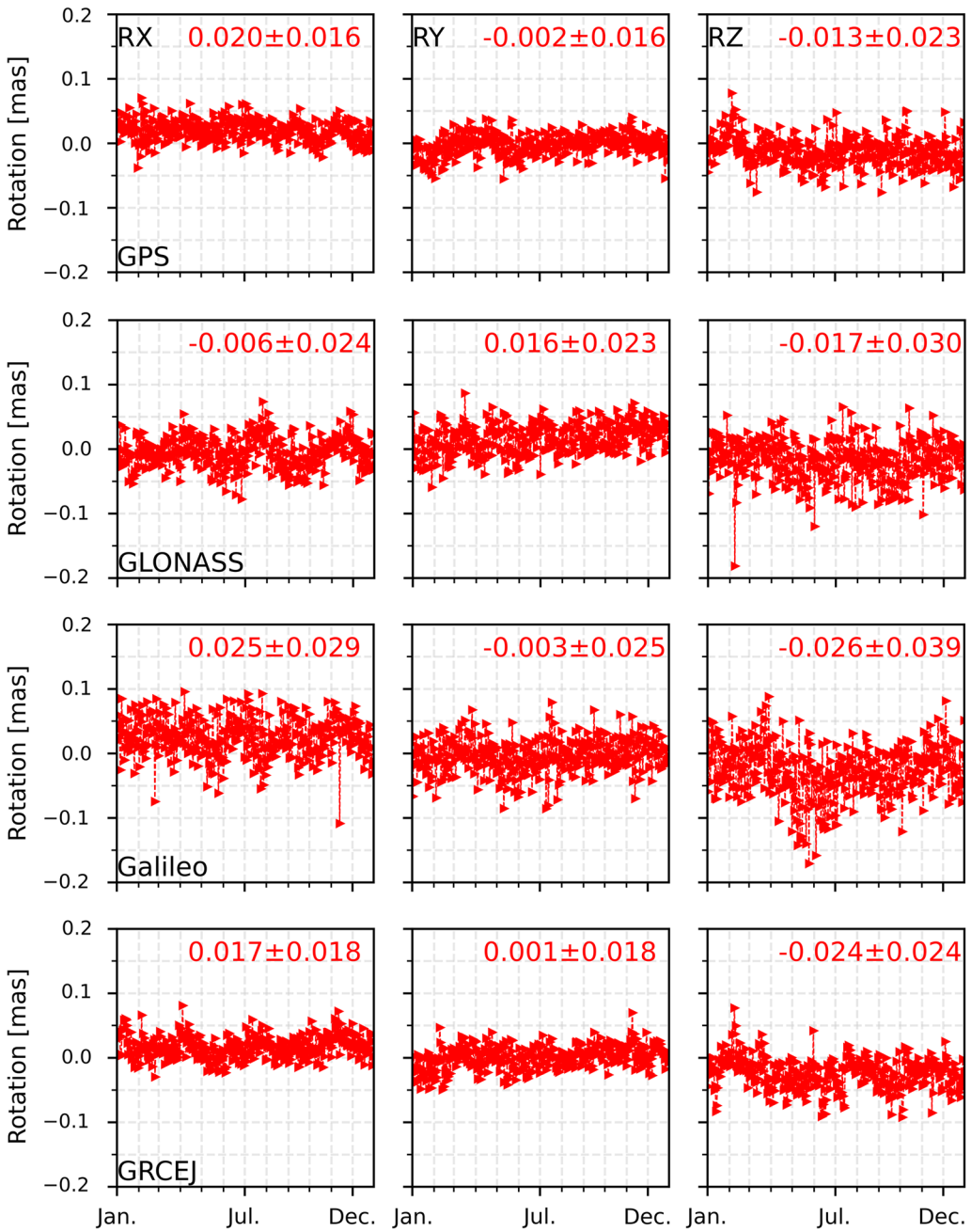

Fig. 10 Rotations of PPP solutions determined with combined orbit and clock solutions with respect to that of the IGS final solution

scale for the combined clocks. Befitted from the proposed strategy of clock combination (i.e., WMC clocks), an improvement of 0.2, 0.1 and 0.6 cm are obtained for the east, north and up component, respectively.

For kinematic PPP of station STK2 with combined clocks without consideration of ASB and nonlinear variations (i.e., RAW clocks), an obvious fluctuation occurs at the time between the 6th and 10th hour in the up component (Fig. 13). Compared to the PPP with RAW clocks, a notable decrease of RMS is obtained in the up component for PPP with WMC clocks, and the RMS of position residuals are 0.8, 0.9 and 2.0 cm for the three components.

Table 6 summarizes the statistic results of PPP tests with single and integrated constellations. Due to insufficient satellites available to conduct Galileo-only and

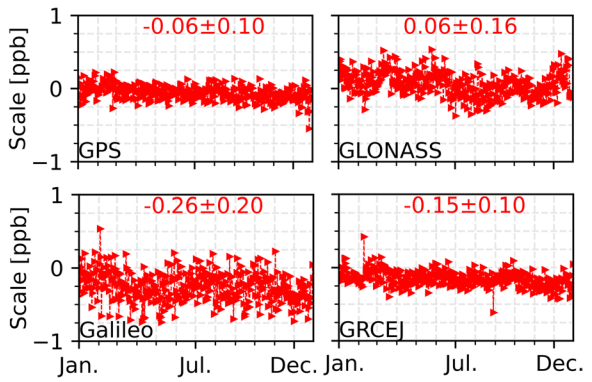

Fig. 11 Scale parameters for single and multi-GNSS PPP solutions with respect to IGS daily coordinates

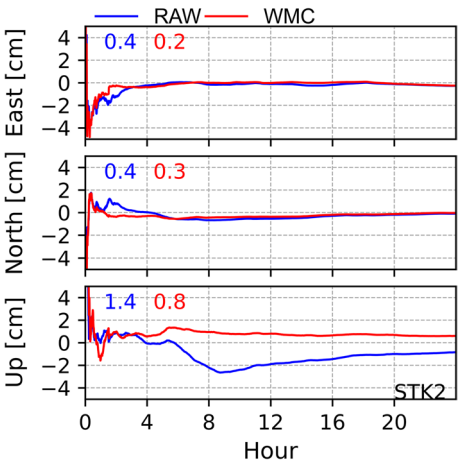

Fig. 12 Positioning error in the earth, north, and up components of multi-GNSS integrated PPP in static mode on January 1, 2018 for station STK2. 'RAW' indicates the PPP results using combined clocks without consideration of ASB and nonlinear variations, and the values in different colors indicate the RMS of position residuals

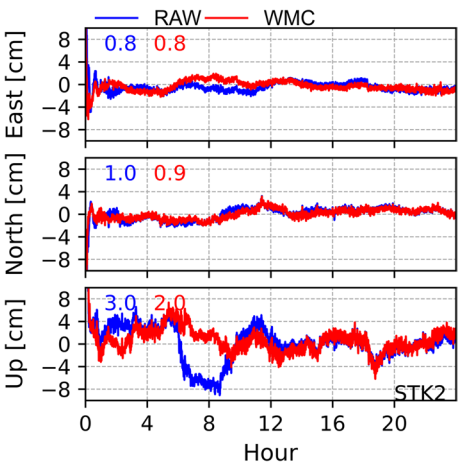

Fig. 13 Positioning error in the east, north, and up components of multi-GNSS integrated PPP in kinematic mode on January 1, 2018 for station STK2

BDS-only PPP, only the single-constellation PPP results of GPS and GLONASS are presented. Compared to the PPP results with RAW clocks, the average improvement of GPS-only positioning accuracy in the three components is less than 6% (i.e., 5.7% for static mode) for PPP with WMC clocks. However, the average improvement could reach 11.1% for GLONASS-only PPP in static mode, which can be explained by the optimal weights designed for ACs when ASB and nonlinear variations in RAW clocks are considered. Compared to the PPP results of individual constellation, the multi-GNSS integrated PPP with WMC clocks in static mode achieves the smallest positioning errors, and the RMS values are 0.63, 0.36 and 1.77 cm in east, north and up components, respectively. The smallest positioning error is also obtained for PPP in kinematic mode, and the corresponding RMS are 1.63, 1.16 and 3.82 cm in the three components. Compared to the results of PPP with RAW clocks, a slight decrease of RMS is found for multi-GNSS PPP with WMC clocks, and average improvements of 9.8 and 5.3% are achieved for PPP in static and kinematic mode, respectively. It could be explained by the fact that the inconsistent nonlinear variation within multi-GNSS in RAW clocks could not be compensated by the daily constant ISB estimates.

Discussion and conclusions

Multi-GNSS combined clocks are derived with solutions from IGS MGEX ACs and ESA for the whole year of 2018. The inconsistent ASB and nonlinear variation induced by the time scale and nonconstant ISB estimates are addressed in this study to achieve reliable clock combination.

Hauschild et al. (2019) pointed out that satellite clock products suffer from chip shape distortions in the ranging signals when the clocks are determined by a network with mixed receivers. As IGS stations with different receivers are used by ACs for precise orbit and clock determination, the analysis center and satellite-specific bias is prone to contaminating the satellite clock solution. Fortunately, this bias can be calibrated with the proposed approach, and a high consistency between the clock and ASB difference is found.

Two factors are identified in the inconsistent nonlinear variation in clock solutions in this study: one is the time scale, and the other one is the nonconstant ISB estimated in clock computation. Since an arbitrary time scale (e.g.,

Table 5 Statistics of the transformation parameters for multi-GNSS integrated PPP with respect to IGS daily coordinates. 'WMC' indicates a PPP solution using the combined orbit and clock

Solution	DX mm	DY mm	DZ mm	RX uas	RY uas	RZ uas	Scale ppb
COM	−0.2 ± 1.0	−1.8 ± 1.2	0.8 ± 1.1	21 ± 19	13 ± 23	−30 ± 29	−0.32 ± 0.18
ESM	−0.6 ± 0.9	−0.3 ± 0.8	−0.2 ± 0.9	15 ± 17	8 ± 17	−13 ± 24	−0.20 ± 0.10
GFM	0.1 ± 0.8	−1.0 ± 0.9	−0.9 ± 0.9	24 ± 18	20 ± 19	15 ± 32	−0.11 ± 0.11
GRM	1.2 ± 1.1	−0.8 ± 1.1	−1.5 ± 1.2	79 ± 21	7 ± 25	29 ± 61	−0.13 ± 0.14
JAM	0.6 ± 1.2	−0.3 ± 1.4	0.8 ± 1.6	3 ± 26	48 ± 32	−49 ± 32	−0.00 ± 0.10
WUM	−0.6 ± 1.8	−0.1 ± 2.3	−3.8 ± 2.6	17 ± 38	−4 ± 39	−1 ± 43	−0.13 ± 0.10
WMC	−0.2 ± 0.8	−0.8 ± 1.0	−0.7 ± 1.0	17 ± 18	1 ± 18	−24 ± 24	−0.15 ± 0.10

Table 6 Average RMS of static/kinematic positioning errors for global stations using combined orbits and clocks

Constellation	RAW (cm)			WMC (cm)		
	East	North	Up	East	North	Up
GPS	0.95/2.71	0.46/1.71	1.95/4.97	0.93/2.59	0.40/1.71	1.91/4.92
GLONASS	0.89/5.92	0.51/2.97	1.98/8.05	0.73/5.54	0.46/2.87	1.87/7.71
ALL	0.69/1.70	0.42/1.27	1.89/3.94	0.63/1.63	0.36/1.16	1.77/3.82

a reference station clock) is usually selected for the satellite clock solution, inconsistent nonlinear variations from the reference clock are common for all satellites and can also be extracted from the average of the fitting residuals. However, the inconsistent nonlinear variations induced by the second factor are always constellation dependent and can only be eliminated by aligning the clocks to a reference solution. With respect to modeling the ISB as a constant, estimating the ISB with a random walk can achieve better positioning accuracy (Liu et al. 2019). Once the ISBs are estimated with a random walk for all ACs, there is no reference clock to be selected for the calibration of the nonlinear variations. Hence, a temporal ISB should be added in the current ASB calibration approach for the correction of inconsistent nonlinear variations.

With respect to the combined solution, the inter-AC clock agreement is 8–16, 27–58, 13–27 and 9–36 ps for GPS, GLONASS, BDS-2 and Galileo, respectively. Outliers up to several nanoseconds sometimes occur for ACs, which demonstrates the necessity of clock combination. The analysis center and constellation-specific weight based on clock residuals is limited by a large ASB, which can be calibrated using the proposed approach. When the ASB is corrected, the RMS of the AC clock residuals obviously decreases, and consistencies of 14–26, 37–91, 33–48 and 12–44 ps for GPS, GLONASS, BDS-2 and Galileo, respectively, are obtained. The average RMS of the ASB residuals also decreases from 46 to 19, from 100 to 34, from 667 to 86 and from 85 to 13 ps for GPS, GLONASS, BDS-2 and Galileo, respectively.

Daily static PPP with float ambiguity was performed for different constellations to assess the combined multi-GNSS orbit and clock while addressing the positioning accuracy and reference frame consistency with regard to the IGS terrestrial frame. For individual constellations, the best position accuracies of 0.31, 0.17 and 0.46 cm in the east, north and up directions, respectively, are achieved for GPS. The position accuracy of the east component is improved by approximately 1 mm for multi-GNSS integrated PPP. The consistency of the combined orbit and clock is also validated by the correlation between translations. However, marginal correlations and offsets of 0.1–0.3 ppb are identified for the scale parameter within the PPP results of different constellations due to inconsistent observational and dynamic models. Generally, the combined multi-GNSS orbit/clock shows competitive performance with that of the best AC in both positioning accuracy and reference frame parameters.

Further improvements are expected as an increasing number of ACs provide multi-GNSS orbits, clocks and other related precise products (e.g., attitudes), and an improved orbit model and consistent correction could also benefit the combined solution. The history of multi-GNSS combined orbit/clock solutions since 2018 will be generated in the near future.

Abbreviations
AC: Analysis center; ACC: Analysis center coordinator; ASB: Analysis center and satellite-specific bias; BDS: BeiDou Satellite Navigation System; EOP: Earth Orientation Parameter; GNSS: Global Navigation Satellite System; IFCB: Inter-frequency code bias; iGMAS: International GNSS Monitoring and Assessment System; IGS: International GNSS Service; IRC: Integer recovery clocks; ISB: Inter-system bias; MGEX: Multi-GNSS Pilot Project; PPP: Precise point positioning; PPP-AR: PPP with Integer Ambiguity Resolution; PNT: Positioning, navigation and timing; RMS: Root mean square; STDev: Standard deviation.

Acknowledgements
The IGS MGEX and its analysis centers are greatly acknowledged for providing the multi-GNSS products and observations.

Author contributions
All the authors contributed to the design of this study. Guo Chen and Qile Zhao came up with the idea. Guo Chen processed the clock combination experiments, generated the results and wrote the draft. Jing Guo revised the manuscript, Na Wei participated in the analysis of transformation parameters, Min Li and Jun Tao participated in collection of MGEX orbit and clock products, and carried out the precise point positioning. All authors read and approved the final manuscript.

Authors' information
Guo Chen is a postdoctoral researcher at GNSS Research Center of Wuhan University. He received his PhD degree at Wuhan University in 2019. His current research mainly focuses on multi-GNSS products combination and performance evaluation.
Jing Guo is an associate professor at GNSS Research Center of Wuhan University. He received his doctor degrees at Wuhan University in2014, and worked as research associate at Newcastle University in 2017. Currently, he works on GNSS data processing, particularly the precise orbit determination for GNSS satellites, and is also responsible for the routine data processing of IGS MGEX and iGMAS at Wuhan University.
Na Wei is an associate professor at GNSS Research Center of Wuhan University. She received her PhD degree at Wuhan University in 2011. Her current research mainly focuses on reference frame and surface loading.
Min Li received a Ph.D. degree from Wuhan University in 2011. He is currently a professor of GNSS Research Center of Wuhan University, and his main work focuses on GNSS satellite orbit determination and multi-GNSS positioning.
Qile Zhao is a professor of GNSS Research Center of Wuhan University. He received his PhD degree at Wuhan University in 2004. His current research interests are precise orbit determination of GNSS and low Earth orbit satellites, and multi-GNSS high-precision positioning.
Jun Tao received his master's degree from Wuhan University, Wuhan, China, in 2019, where is currently a Ph.D. candidate at the School of Geodesy and Geomatics. His main research interest is real-time GNSS positioning and its application.

Funding
This work was supported by National Natural Science Foundation of China (41974035, 42030109, 42204019), Young elite scientists sponsorship program by CAST (2018QNRC001) and Fundamental Research Funds for the Central Universities (2042021kf0064).

Availability of data and materials
Multi-GNSS precise orbits and global station observations are available by an anonymous user via ftp://igs.gnsswhu.cn. The precise products of ESA can be obtained from http://navigation-office.esa.int/products. The combined orbit and clock solutions can also be freely accessed at ftp://igs.gnsswhu.cn/whu/MGEX.

Declarations

Competing interests
The authors declare that no conflicts of interest associated with this publication.

Author details
[1]GNSS Research Center, Wuhan University, No. 129 Luoyu Road, Wuhan 430079, China. [2]Collaborative Innovation Center of Geospatial Technology, Wuhan University, No. 129 Luoyu Road, Wuhan 430079, China. [3]School of Geodesy and Geomatics, Wuhan University, No. 129 Luoyu Road, Wuhan 430079, China.

Received: 3 May 2022 Accepted: 2 September 2022
Published online: 19 September 2022

References
Banville S, Geng J, Loyer S, Schaer S, Springer T, Strasser S (2020) On the interoperability of IGS products for precise point positioning with ambiguity resolution. J Geod 94:10. https://doi.org/10.1007/s00190-019-01335-w
Beutler G, Mueller II (1994) Neilan RE (1994) The International GPS Service for Geodynamics (IGS): development and start of official service on January 1. Bull Geod 68(1):39–70
Beutler G, Kouba J, Springer T (1995) Combining the orbits of the IGS analysis centers. Bull Geod 69:200–222
Chen K, Xu T, Chen G, Li J, Yu S (2015) The Orbit and Clock Combination of iGMAS Analysis Centers and the Analysis of Their Precision. In: Sun J, Liu J, Fan S, Lu X (eds) China Satellite Navigation Conference (CSNC) 2015 Proceedings: Volume II Lecture Notes in Electrical Engineering, vol II. Springer, Berlin
Chen K, Xu T, Yang Y (2017) Robust combination of IGS analysis center GLONASS clocks. GPS Solut 21:1251–1263. https://doi.org/10.1007/s10291-017-0610-0
Dach R, Schaer S, Arnold D, Prange L, Sidorov S, Sušnik A, Stebler P, Villiger A, Jäggi A, Beutler G, Brockmann E, Ineichen D, Lutz S, Wild U, Nicodet M, Dostal J, Thaller D, Söhne W, Bouman J, Selmke I, Hugentobler U (2019) Center for Orbit Determination in Europe (CODE) Technical Report 2018. In: Villiger A, Dach R (eds). International GNSS Service Technical Report 2018 (IGS Annual Report). Bern: IGS Central Bureau and University of Bern
Dow JM, Neilan RE, Rizos C (2009) The international GNSS service in a changing landscape of global navigation satellite systems. J Geodesy 83(3):191–198. https://doi.org/10.1007/s00190-008-0300-3
Ferland R (1999) Densification of ITRF, reference frame working group report, 1998 IGS technical reports. Pasadena, Jet Propulsion Laboratory, pp 219–222
Geng J, Chen X, Pan Y, Zhao Q (2019) A modified phase clock/bias model to improve PPP ambiguity resolution at Wuhan University. J Geod 93:2053–2067
Griffiths J (2019) Combined orbits and clocks from IGS second reprocessing. J Geod 93:177–195. https://doi.org/10.1007/s00190-018-1149-8
Hauschild A, Steigenberger P, Montenbruck O (2019) Inter-receiver GNSS pseudorange biases and their effect on clock and DCB estimation Proc. ION GNSS 2019. Institute of Navigation, Miami, pp 3675–3685
Kouba J, Héroux P (2001) GPS precise point positioning using IGS orbit products. GPS Solut. 5(2):12–28. https://doi.org/10.1007/PL00012883
Kouba J, Mireault Y, Lahaye Y (1995) 1994 IGS orbit/clock combination and evaluation, appendix I of the analysis coordinator report, international GPS service for geodynamics (IGS) 1994 annual report, pp 70–94
Kouba J, Springer T (2001) New IGS station and satellite clock combination. GPS Solut 4(4):31–36. https://doi.org/10.1007/PL00012863
Kouba J (2000) IGS orbit/clock navigation & sat. clock interpolations with no SA, [IGSMAIL-2824]. https://lists.igs.org/pipermail/igsmail/2000/004197.html
Liu J, Ge M (2003) PANDA Software and Its Preliminary Result of Positioning and Orbit Determination. Wuhan Univ J Nat Sci 8(2):603–609. https://doi.org/10.1007/BF02899825
Liu X, Jiang W, Chen H, Zhao W, Huo L, Huang L, Chen Q (2019) An analysis of inter-system biases in BDS/GPS precise point positioning. GPS Solut 23:116. https://doi.org/10.1007/s10291-019-0906-3
Loyer S, Banville S, Perosanz F, Mercier F (2017) Disseminating GNSS satellite attitude for improved clock correction consistency. IGS Workshop 2017

Loyer S, Banville S, Geng J, Strasser S (2021) Exchanging satellite attitude quaternions for improved GNSS data processing consistency. Adv Space Res 68(6):2441–2452. https://doi.org/10.1016/j.asr.2021.04.049
Masoumi S, Moore M (2019) IGS ACC v2.0-Status of the software. Unified Analysis Workshop, 4 October, 2019, Paris, France
Mervart L, Weber G (2011) Real-time combination of GNSS orbit and clock correction streams using a Kalman filter approach Proceedings of ION GNSS-2011. Institution of Navigation, Portland, pp 707–711
Montenbruck O et al (2017) The Multi-GNSS Experiment (MGEX) of the International GNSS Service (IGS)—achievements, prospects and challenges. Adv Space Res 59:1671–1697
Pan Y (2021) BDS/GNSS Clock and Phase Bias Products Combination for Precise Point Positioning with Ambiguity Resolution. (M): Wuhan University (in Chinese)
Perosanz F, Loyer S, Mercier F, Katsigianni G, Mezerette A, Capdeville H, Versini L, Marty JC, Santamaria A (2018) CNES-CLS Technical Report 2018. In: Villiger A, Dach R (eds) International GNSS Service Technical Report 2018 (IGS Annual Report). IGS Central Bureau and University of Bern, Bern
Petit G, Arias EF (2009) Use of IGS products in TAI applications. J Geod 83:327–334
Ray JR (1999) IGS/BIPM time transfer pilot project. GPS Solut 2(3):37–40. https://doi.org/10.1007/PL00012755ImpSenior K (2001) [IGSMAIL-3615]: IGS time scale. https://lists.igs.org/pipermail/igsmail/2001/004988.html
Sakic P, Mansur G, Viegas E, Männel B (2018) Schuh H (2018) Towards a Multi-Constellation combination: improving the IGS orbit & clock combination software for MGEX products. IGS workshop, Wuhan
Schaer S, Villiger A, Arnold D, Dach R, Prange L, Jäggi A (2021) The CODE ambiguity-fixed clock and phase bias analysis products: generation, properties, and performance. J Geod 95:81
Song W, Yi W, Lou Y, Shi C, Yao Y, Liu Y, Mao Y, Xiang Y (2014) Impact of GLONASS pseudorange inter-channel biases on satellite clock corrections. GPS Solut 18:323–333. https://doi.org/10.1007/s10291-014-0371-y
Sośnica K, Zajdel R, Bury G, Bosy J, Moore M, Masoumi S (2020) Quality assessment of experimental IGS multi-GNSS combined orbits. GPS Solut 24:54. https://doi.org/10.1007/s10291-020-0965-5
Springer T, Beutler G (1993) Towards an official IGS orbit by combining the results of all IGS Processing Centers Proceedings of the IGS Workshop. Bern: University of bern, pp. 24–26
Zhao Q, Guo J, Liu S, Tao J, Hu Z, Chen G (2021) A variant of raw observation approach for BDS/GNSS precise point positioning with fast integer ambiguity resolution. Satell Navig. https://doi.org/10.1186/s43020-021-00059-7
Zumberge JF, Heflin MB, Jefferson DC, Watkins MM (1997) Precise point positioning for the efficient and robust analysis of GPS data from large networks. J Geophys Res 102(B3):5005–5017. https://doi.org/10.1029/96JB03860

Publisher's Note